

# Geophysical Research Letters<sup>®</sup>



## RESEARCH LETTER

10.1029/2021GL095879

### Key Points:

- Corona discharges at cloud tops form a distinct type of electric discharges with rise times  $<20 \mu\text{s}$  in 337 nm and little activity in 777.4 nm
- They are generated both in developing storm cells overshooting the tropopause height and collapsing cells with remaining convective activity
- Most are detected by ground-based lightning detection systems implying they are fast break-down discharges with high currents

### Supporting Information:

Supporting Information may be found in the online version of this article.

### Correspondence to:

K. Dimitriadou,  
[krstd@space.dtu.dk](mailto:krstd@space.dtu.dk)

### Citation:











Dimitriadou, K., Chanrion, O., Neubert, T., Protat, A., Louf, V., Heumesser, M., et al. (2022). Analysis of blue corona discharges at the top of tropical thunderstorm clouds in different phases of convection. *Geophysical Research Letters*, 49, e2021GL095879. <https://doi.org/10.1029/2021GL095879>

Received 2 SEP 2021  
Accepted 27 FEB 2022

© 2022. The Authors.

This is an open access article under the terms of the [Creative Commons Attribution-NonCommercial-NoDerivs License](https://creativecommons.org/licenses/by-nc-nd/4.0/), which permits use and distribution in any medium, provided the original work is properly cited, the use is non-commercial and no modifications or adaptations are made.

## Analysis of Blue Corona Discharges at the Top of Tropical Thunderstorm Clouds in Different Phases of Convection

Krystallia Dimitriadou<sup>1</sup> , Olivier Chanrion<sup>1</sup> , Torsten Neubert<sup>1</sup> , Alain Protat<sup>2</sup> ,  
Valentin Louf<sup>2</sup> , Matthias Heumesser<sup>1</sup> , Lasse Husbjerg<sup>1</sup> , Christoph Köhn<sup>1</sup> ,  
Nikolai Østgaard<sup>3</sup> , and Victor Reglero<sup>4</sup> 

<sup>1</sup>National Space Institute, Technical University of Denmark (DTU Space), Kongens Lyngby, Denmark, <sup>2</sup>Australian Bureau of Meteorology, Science and Innovation Group, Radar Science and Nowcasting Team, Melbourne, VIC, Australia, <sup>3</sup>Birkeland Centre for Space Science, University of Bergen, Bergen, Norway, <sup>4</sup>Image Processing Laboratory, University of Valencia, Valencia, Spain

**Abstract** We report on observations of corona discharges at the uppermost region of clouds characterized by emissions in a blue band of nitrogen molecules at 337 nm, with little activity in the red band of lightning leaders at 777.4 nm. Past work suggests that they are generated in cloud tops reaching the tropopause and above. Here we explore their occurrence in two convective environments of the same storm: one is developing with clouds reaching above the tropopause, and one is collapsing with lower cloud tops. We focus on those discharges that form a distinct category with rise times below  $20 \mu\text{s}$ , implying that they are at the very top of the clouds. The discharges are observed in both environments. The observations suggest that a range of storm environments may generate corona discharges and that they may be common in convective surges.

**Plain Language Summary** Discharges in thunderstorm clouds with little or no lightning leader emissions are from cold streamers and are called corona discharges. They are thought to be generated in the upper regions of clouds that may reach into the stratosphere. Here we explore if storms with lower cloud tops may also generate these by comparing measurements of a collapsing and a developing thunderstorm environment that are part of a larger storm system. We find that the discharges are created in both environments and, therefore, may be quite common.

## 1. Introduction

Blue electrical discharges may form at the top of thunderstorm clouds. They include those that propagate upwards into the stratosphere to  $\sim 40\text{--}50$  km such as blue starters and blue jets and those that remain close to the cloud such as the pixies, gnomes and km-scale corona discharges (Chanrion et al., 2017; Krehbiel et al., 2008; Liu et al., 2015; Lyons et al., 2003; Wescott et al., 1995). Unlike optical emissions in the mesosphere (sprites, elves), they are difficult to detect from the ground because the clouds obstruct the view and the blue light is absorbed and scattered by the troposphere. Therefore, studies are often based on observations from space that allow for an unimpeded view of the discharges (Chanrion et al., 2017; Chou et al., 2010; Kuo et al., 2009; Neubert et al., 2021).

The meteorological environments that produce blue corona discharges are usually moist tropical and mid-latitude thunderstorms with single-cell or multi-cell formation (Li et al., 2021; Liu et al., 2018; Neubert et al., 2021; Soler et al., 2020). Some tend to originate near overshooting tops of convective clouds, thus representing a coupling between the troposphere and the stratosphere, powered by the underlying convective activity (Chanrion et al., 2017; Liu et al., 2021). It appears that they occur during the developing or mature stage of a storm; however, observations are scarce. Therefore, we have analyzed optical and ultraviolet (UV)-measurements by the Atmospheres-Space Interactions Monitor (ASIM) as it passed over a thunderstorm in the region of Darwin, Australia, during the southern hemisphere summer. The storm is interesting because it includes a developing region with cloud tops reaching the tropopause and above and a dissipating region with lower cloud tops.

Blue corona discharges in clouds are of a few tens of microsecond duration and are characterized by the absence of lightning leader emissions, commonly measured in a narrow band around the atomic oxygen line at 777.4 nm (Christian et al., 1989). They are, therefore, emissions from cold streamers and are sometimes referred to as streamer coronae (Soler et al., 2020). Corona emissions observed from space may appear with a range of rise times that reflect the amount of photon scattering by cloud particles. The rise time, therefore, is a measure of

the depth in clouds of the discharges. The polarity of the discharges depends on the polarity of the charge layers where they originate. Discharges some kilometers below the cloud tops have been related to positive polarity narrow bipolar events (NBEs), which are signatures in electromagnetic waveform data in the frequency range 3–300 MHz that have a brief duration of 10–30  $\mu$ s (Soler et al., 2020; Wu et al., 2012). Blue discharges at the cloud tops have been associated with negative NBEs (Chou et al., 2018; Liu et al., 2018, 2021), generated in the regions of the upper positive charge layer and the negative screening layer above it. NBEs may mark the onset of lightning (Tilles et al., 2019) and blue jets to the stratosphere (Neubert et al., 2021).

The analysis we present in this paper is focused on the cloud-top discharges with short rise times. We first present the methodology and data sources of the study, then the observations and analysis, and finally a discussion.

## 2. Data Sources and Methods

Atmospheres-Space Interactions Monitor on the International Space Station (ISS) is a suite of nadir-pointing instruments for measurements of conventional lightning, Transient Luminous Events and Terrestrial Gamma-ray Flashes (Neubert et al., 2019). It includes three photometers measuring in 337.0/4 nm (blue), 180–230 nm (UV) and 777.4/5 nm (red), with a temporal resolution of 100 kHz, and two cameras in 337.0/5 nm and 777.4/3 nm running at up to 12 frames per second with a spatial resolution of 400–500 m on the ground. The blue band is associated with  $N_2P$ , one of the strongest emissions in discharges. Because the UV band is strongly absorbed in the atmosphere, signals in the UV photometer are used to identify emissions in the stratosphere, mesosphere and lower ionosphere (blue jets, sprites, elves). The red band selects the main emission line of lightning leaders emitted by atomic oxygen. If more than two instruments trigger on a flash, the data are saved for downlink (Chanrion et al., 2019).

During the  $\sim$ 1.5 min overpass of the storm, we find that events with rise times in the blue photometer signal below 20  $\mu$ s and the ratio of the red/blue pulses peaks below 0.15 form a distinct group. The short rise time signifies the emissions are almost unaffected by cloud scattering and that the source altitudes are less than  $\sim$ 1 km below the cloud top (see Supporting Information S1 for details). The dominance of the blue emissions suggests they primarily are streamer flashes associated with weak leader activity. We focus our analysis on these events and we will refer to them as blue corona discharges.

We use lightning data from the Global Lightning Detection network (GLD360) (Said et al., 2013) and the Earth Networks Total Lightning Network (ENTLN) (Marchand et al., 2019) to characterize the temporal evolution of the electric activity of the thunderstorm regions and to correlate them with the blue corona discharges. In addition, we correlate the absolute timing of the ASIM data to  $\sim$ 1 ms accuracy by aligning the red photometer pulses with the GLD360 strokes. Here we neglected the propagation delay of photons from the lightning source to the detector since the important aspect is the correct correspondence of optical pulses measured by ASIM with lightning sources detected by ground-based networks.

The geographic location of the blue corona discharges is estimated by projecting the camera images to 16 km altitude, which is taken as a reference altitude of the cloud tops. The accuracy depends primarily on the accuracy of the location and attitude of the ISS, and the mounting precision of the sensors. It is estimated to be better than  $\sim$ 20 km. The median of the GLD accuracy is 1.8 km and a 90th percentile error is 6.4 km (Said & Murphy, 2016).

We characterize the meteorological context of the storm with measurements of the brightness temperature (BT) from the Himawari-8 geostationary satellite. The data is supplied by the Japan Aerospace Exploration Agency (JAXA) and updates every 10 min with a spatial resolution of 2 km (Bessho et al., 2016). The cloud top temperature (CTT) and the cloud top height (CTH) are estimated by translating the BT to CTT and then to CTH using atmospheric sounding data provided by the University of Wyoming. The closest temperature profile was taken from station 94,120 YPDN at Darwin Airport ( $-12.42^\circ$ ,  $130.89^\circ$ ). The structure and vertical extent of the storm are derived from reflectivity data from a single-polarization Doppler C-band weather radar in Berrimah, Northern Australia ( $-12.46^\circ$ ,  $130.93^\circ$ ). It gives a full 3D volumetric scan every 6 min using 13 elevation angles ( $0.5^\circ$ – $32^\circ$ ). These volumetric observations are then gridded at a resolution of 1 km horizontally and 500 m vertically. The radar makes 3D volumetric scans with 150 km range, and an additional quasi-horizontal “surveillance” scan with 250 km range.

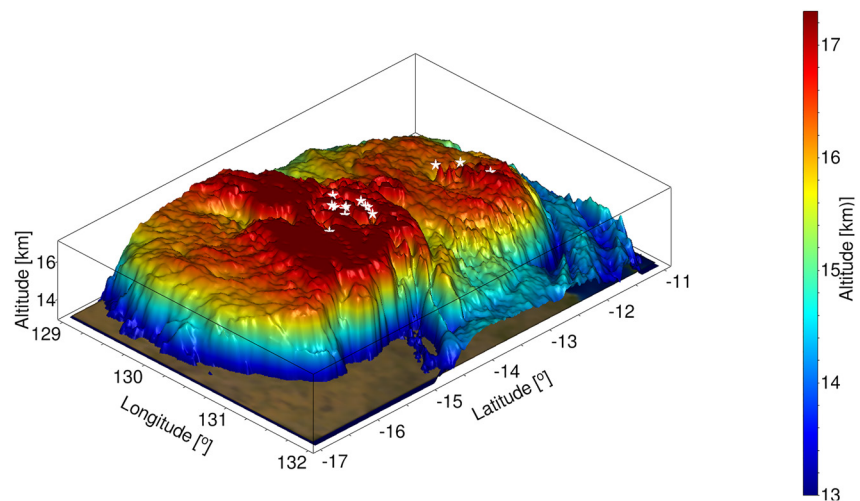


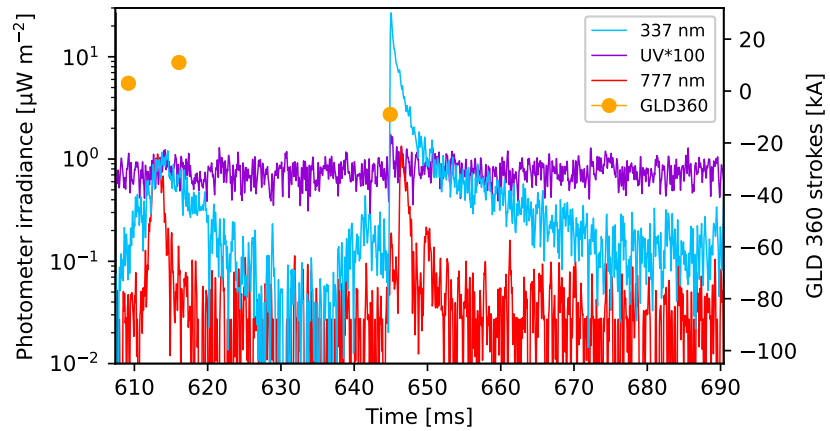
**Figure 1.** The cloud top altitude of the multi-cell thunderstorm over Northern Australia on 30 January 2021 at 17:00 Universal Time Coordinated. The altitude is reconstructed by the Himawari satellite and the atmospheric sounding. The white stars are the position of the blue corona discharges, obtained by projection of the Atmospheres-Space Interactions Monitor data to 16 km altitude.

### 3. Observations and Analysis

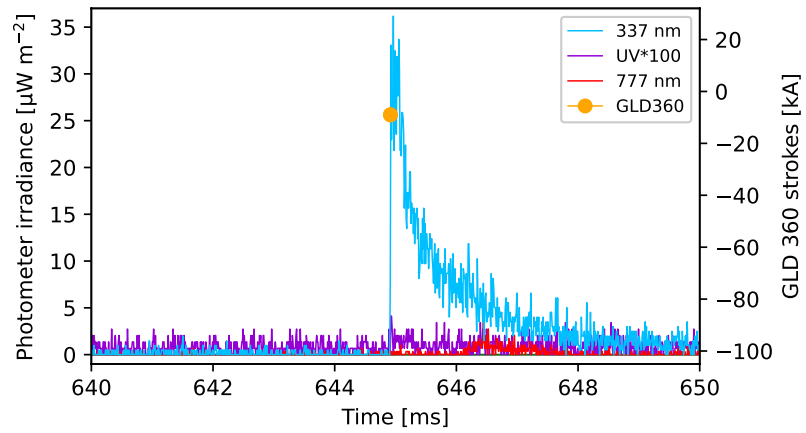
The north-western part of Australia is characterized by frequent thunderstorms with heavy rainfall and intense lightning, especially over land (Laroche et al., 2009). This region has the highest number of lightning days in all the Australian territories during 2004–2013 (Bates et al., 2017). ASIM passed over a storm in the region on 30 January 2019, between 17:02:12.519 and 17:03:43.695 Universal Time Coordinated (UTC). Infrared satellite measurements identified two large groups of cells, a northern one with cloud tops at 15–17 km (above  $-13.1^{\circ}$  latitude) and a southern one with cloud tops at 16–17+ km. They are shown in Figure 1 at 17:00 UTC. The storm began to form the day before and developed into a tropical multi-cellular thunderstorm as it moved towards the Northwest. The atmospheric sounding (Figure S1 in the Supporting Information S1) closest in space and time was at 12:00 UTC. It reported very humid conditions with nearly saturated air between the cloud base ( $\sim 500$  m) and the tropopause ( $\sim 17.05$  km) as well as extreme instability with a Convective Available Potential Energy (CAPE) of  $4000 \text{ J kg}^{-1}$ . The equilibrium level was at 17.15 km, meaning that an ascending air parcel could continue moving upwards above the tropopause layer. At the time of the overpass, the northern cells were dissipating and the southern cells were growing (Figure S2 in the Supporting Information S1). The electrical activity was decreasing in the dissipating cells and increasing in the growing cells (Figures S3 and S4 in the Supporting Information S1). There was a substantial wind shear with strong winds from the west and south below 7.5 km and strong winds from the east further above. This wind profile strengthens the storm since it displaces the updraft from the downdraft, thus allowing updraft motions to be sustained for a longer time. The wind speed increased from  $\sim 18$  knots at 13.7 km ( $\sim 163$  hPa) to  $\sim 70$  knots at the tropopause ( $\sim 91$  hPa).

The instrument triggered a total of 134 times during the overpass. The captured sequences include photometer pulses from conventional lightning where both red and blue signals have significant amplitudes and a multitude of primarily blue pulses with varying rise times. Fourteen pulses that satisfy the criteria of blue corona discharges are from locations in both storm regions, with most in the developing region. The distribution with rise time of all blue corona discharges, including those that are deeper in the clouds, is shown in Figure S5 in the Supporting Information S1.

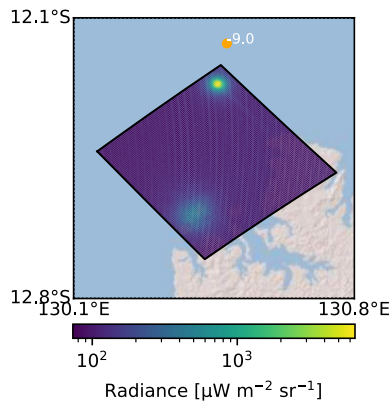
An example of a blue corona discharge is shown in Figure 2. Figure 2a presents the three photometer signals during one camera frame exposure. We see that the blue photometer signal dominates over the red. It has a peak in the middle of the frame with a peak value almost two orders of magnitude stronger than the red signal and fades during the remaining  $\sim 40$  ms of the frame exposure. Figure 2b is a zoom on the event and is on a linear scale to illustrate the short rise time of the blue pulse. The corresponding camera images are at the bottom panels, with the blue image on the left (c) and the red on the right (d). The red emissions in the lower corner of the image



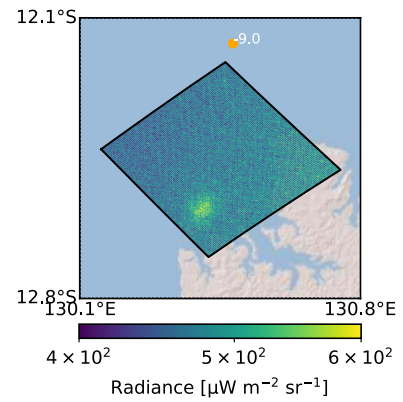
a)



b)



c)



d)

**Figure 2.** Blue corona discharge in a dissipating cell. (a) Photometer signals corresponding to the blue pulse and accompanying ultraviolet and red signals, on logarithmic scale and 5-point Gaussian filtered. Concurrent Global Lightning Detection network (GLD) strokes (dots) displayed on top.  $t = 0$  corresponds to 30 January 2019 17:02:22.441 Universal Time Coordinated. The time range of the photometer matches the exposure time of the respective camera frame ( $\sim 83.3$  ms). (b) Photometer signals around the blue corona discharge, on linear scale and non-filtered. (c) 337.0 nm and (d) 777.4 nm camera images projected on an altitude of 16 km. GLD strokes occurring within the integration time are displayed on top. The display images are the cropped and downloaded Modular Multispectral imaging array images with the observed activity.

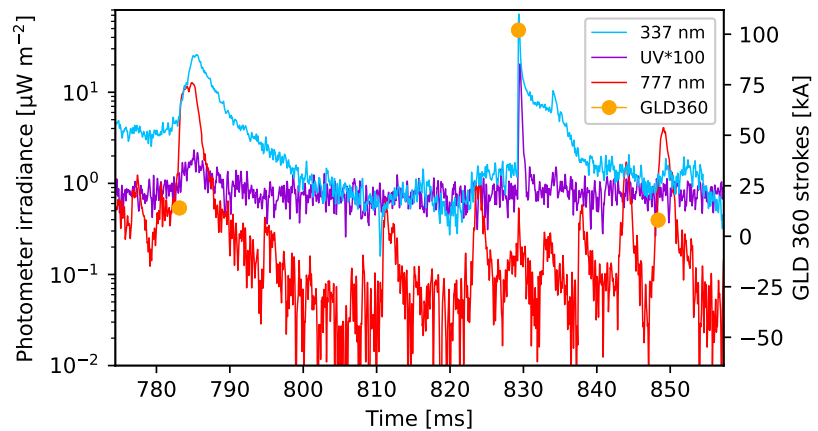
correspond to the weak emissions in the blue image, whereas the blue image includes distinct emissions in the upper corner, not found in the red. The photometer signals then represent two events. We identify the one in the lower corner as a lightning event at some depth in the cloud associated with the red photometer signal and the one in the upper corner associated with the blue pulse. The pulse is in frame 3 of an 8-frame sequence of pulses that primarily are blue (Figure S6 in the Supporting Information S1).

The decay over  $\sim 40$  ms of the blue pulse suggests that the discharge may rise above the cloud, as concluded for a similar event in Neubert et al. (2021). In this case we would expect to see emissions reflected in the cloud and therefore a diffuse region of the cloud surrounding the discharge. This appears to be borne out by the camera image where the blue spot (upper corner) is consistent with a diffuse region of  $\sim 10$  km diameter. A negative stroke of  $-9$  kA, identified by the GLD sensors, appears to be correlated with pre-activity preceding the blue corona discharge. The differences in time and location are  $\sim 0.7$  ms and  $\sim 10$  km, which are within the accuracy of the data. This suggests that the discharge carries a current pulse of a magnitude comparable to weak Intra Cloud lightning currents with a polarity consistent with negative NBEs, for example, the discharge carries positive charge aloft.

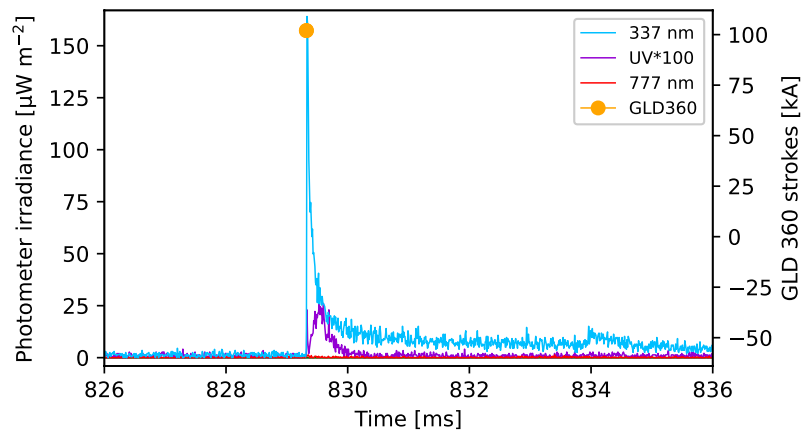
A second example of a blue corona discharge is shown in Figure 3. The signal in the blue band increases two orders of magnitude within  $\sim 20$   $\mu$ s and fades over the following 15–30 ms. A zoom on the event (b) shows that the UV signal reaches its maximum amplitude  $\sim 200$   $\mu$ s after the blue peak. The event is almost identical to one discussed in Neubert et al. (2021), where the UV signal was interpreted as a signature of an elve because of its longer rise time. An elve is a ring of emissions in the lower ionosphere, rapidly expanding to several 100 km radius, powered by the electromagnetic pulse from the current of a lightning stroke below (van der Velde & Montanyà, 2016). The presence of an elve and the absence of significant red emissions suggest that the discharge carries significant currents. This is supported by GLD360 observations of a stroke coincident in time and location (within 9.5 km) with a strong peak current of +102 kA. The polarity is reported as positive whereas elves usually are associated with negative flashes. Furthermore, a positive polarity would suggest a positive NBE usually is found lower in the clouds. The camera images (c,d) show two regions of activity in both images and one exclusively in the blue. The blue region is saturated, seen as an extension of a signal along the direction of a pixel row. The pulse is in frame 4 of an 8-frame sequence (Figure S7 in the Supporting Information S1) that contains both blue- and red-dominated pulses. We identify the blue pulse of the photometer with the blue signal of the camera. However, also in this case, the blue pulse is part of a larger sequence of activity that is quite complex. There are two minor GLD strokes at +14 and +8 kA that correlate with a red peak within  $\sim 1$ –2 ms,  $\sim 9.7$  km. The correlated strokes are shown in Figures 3c and 3d.

The blue corona discharges in Figures 2 and 3 are from the dissipating cloud region (northern) and the developing region (southern), respectively. Their relation to the vertically integrated radar reflectivity is shown in Figure 4a. The integrated reflectivity is the sum of all reflectivities in a column and provides information for the ice part (convective cores) of a reflectivity profile. It also accentuates columns where the reflectivity is strong, meaning that convective cores are better identified. The three discharges in the northern cells are from regions of high reflectivity and cloud tops at  $\sim 15$ –17 km (Figure 1) and the eleven in the southern cells are from regions of moderate to high reflectivity and cloud tops that likely reach above the tropopause, as determined by the reference radiosonde. The northern region is within a range that allows 3D vertical cross sections of the cloud. Figures 4b and 4c are scans along the latitude and longitude of the blue corona discharge in Figure 2. It is located in an area where the radar detects an overshooting top.

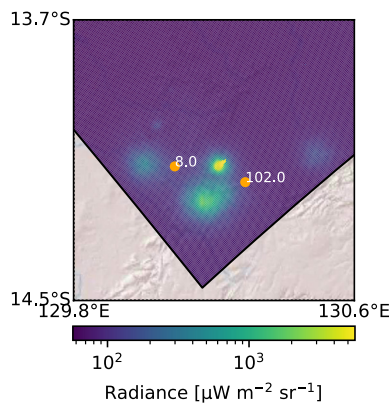
Of the 14 blue corona discharges, 12 correlate with strokes of negative polarity and 2 with positive polarity. The discharges associated with peak amplitudes above 32 kA have a small rise in the UV signal simultaneous to the blue signal with UV/blue amplitude  $\sim 10^{-4}$ . The ratio is consistent with photons from the LBH band, generated by the discharge at the cloud tops, leaking through the absorbing atmosphere to the detector (Neubert et al., 2021). There are 10 discharges in this category, 7 of which have additional UV pulses, as shown in Figure 3, suggesting they generate elves. These are associated with the highest currents as detected by GLD360 ( $> 50$  kA), which may explain the generation of elves. An overview table with the properties associated with the blue corona discharges is shown in the Table S1 in the Supporting Information S1.



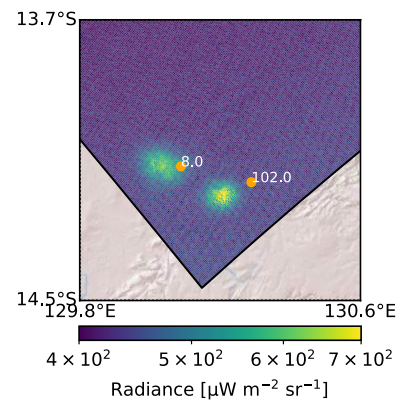
a)



b)



c)



d)

**Figure 3.** Blue corona discharge in a developing cell. (a) Photometer signals corresponding to the blue pulse and accompanying ultraviolet and red signals, on logarithmic scale and 5-point Gaussian filtered. Concurrent Global Lightning Detection network (GLD) strokes (dots) displayed on top.  $t = 0$  corresponds to 30 January 2019 17:02:48.525 Universal Time Coordinated. The time range of the photometer matches the exposure time of the respective camera frame ( $\sim 83.3$  ms). (b) Photometer signals around the blue corona discharge, on linear scale and non-filtered. (c) 337.0 nm and (d) 777.4 nm camera images projected on an altitude of 16 km. GLD strokes occurring within the integration time are displayed on top. The display images are the cropped and downloaded Modular Multispectral imaging array images with the observed activity.

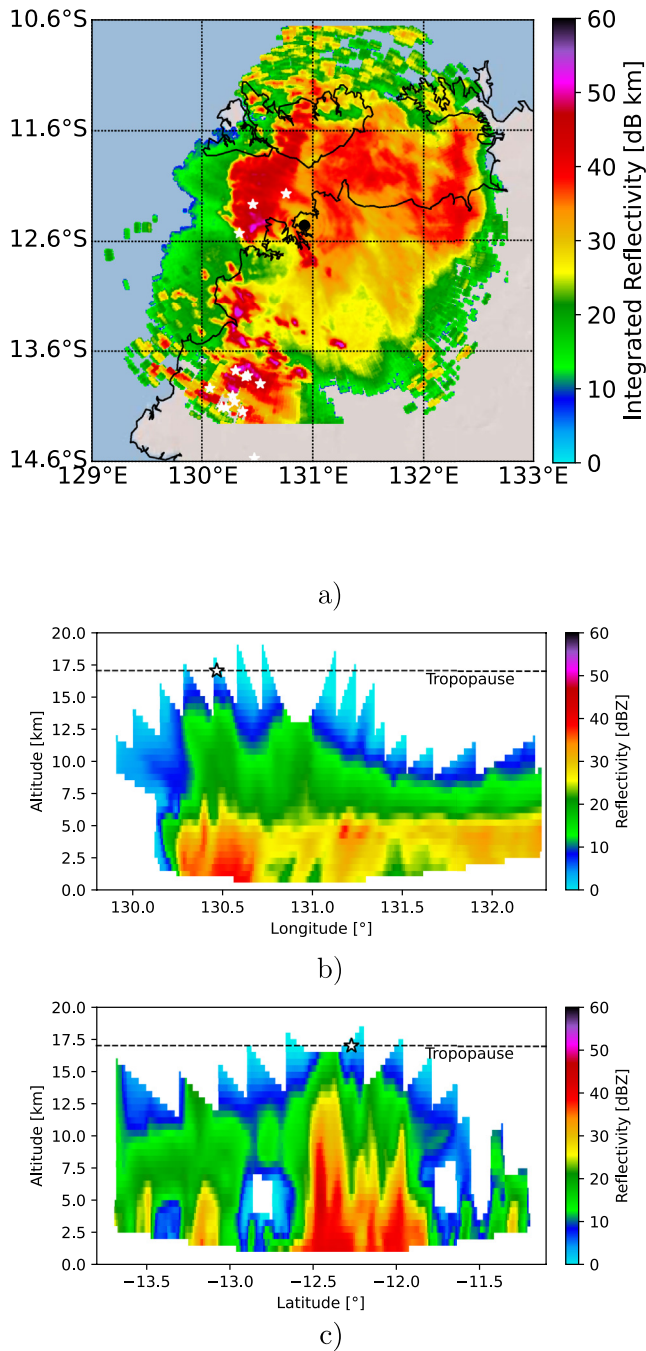


**Figure 4.** (a) The radar integrated reflectivity of the multi-cell thunderstorm over Northern Australia on 30 January 2021 at 17:00:31 Universal Time Coordinated. The white stars indicate the position of the blue corona discharges. (b) The vertical cross sections along  $-12.27^\circ$  latitude. (c) The vertical cross section along  $130.47^\circ$  longitude. The white stars indicate the longitude and latitude of the blue corona discharge. The dashed line shows the altitude of the tropopause as derived by the sounding.

#### 4. Discussion and Interpretation

ASIM detected 14 blue pulses with rise times below  $20 \mu\text{s}$  and a red/blue signal ratio less than 0.15. The short rise time indicates that photons are relatively unaffected by scattering in the cloud and that their sources, therefore, are at the cloud tops. The absence of (or weak) emissions in the red ( $777.4 \text{ nm}$ ) indicates low leader activity, suggesting the emissions primarily are from streamers.

The blue corona discharges are located close to the highest cloud tops in both the collapsing and growing cells. Wiens et al. (2008) demonstrated that reflectivity can be used as a proxy for convection strength and values above 40 dBZ can indicate convective activity. In their study, they use the composite reflectivity, which is the strongest radar echo intensity from any elevation angle and reveals the highest reflectivity in all echoes. In our analysis, we use the integrated reflectivity (the sum of all reflectivities in an atmospheric column) as a more detailed measure of convection strength. The integrated reflectivity for all the blue corona discharges is  $\sim 25\text{--}50 \text{ dB km}$  (Table S1 in the Supporting Information S1). The cells can be rather small, as in the case of the northern, dissipating region (Figure 1), with diameters around the accuracy of the ground projection of the ASIM events ( $\sim 20 \text{ km}$ ). Thus there is some uncertainty on the values of the integrated reflectivity and cloud top altitude associated with a blue corona discharge. An added complexity is that the southern region is relatively far from the radar, which may underestimate the derived integrated reflectivities. In general, higher reflectivities are indicative of larger precipitation particles, and the reflectivity cores observed in the radar cross sections (Figures 4b and 4c) extend upward because hydrometeors are being carried upwards by the intense updrafts. Lower reflectivities can have a lateral extend beyond the core and these regions can be highly electrified (Stolzenburg et al., 1998). Our observations support the notion that developing regions of deep convection with high cloud tops may generate blue corona discharges, but that these are also generated in cloud tops of dissipating convective cells.

The updraft motion of air in clouds facilitates the formation and growth of mixed-phase hydrometeors such as ice crystals, graupel and supercooled droplets. Collisions between these hydrometeors result in electrification processes within the cloud. Clouds need to contain precipitation-size ice particles for electrification processes. Zipser and Lutz (1994) suggested that lightning-producing clouds with reflectivities  $>30 \text{ dBZ}$  above the freezing level indicate the presence of ice. Wu et al. (2012) used this criterion and found that NBE rates increase with the maximum altitude of  $\geq 30 \text{ dBZ}$ . In the storm we present here, the freezing level is around 4.7 km altitude, and the altitude of 30 dBZ is 5–6.5 km in the region of the three blue corona discharges (Figures 4b and 4c, Figures S8 and S9 in the Supporting Information S1). We conjecture then, that although the flash rates (Figures S3 and S4 in the Supporting Information S1) indicate dissipation of convective activity in the southern group of cells, there were enough ice hydrometeors and convection in some of the cells to facilitate the conditions for NBEs, and thereby blue corona discharges.

Blue corona discharges, like those presented here, appear to be the equivalent of negative NBEs (Liu et al., 2021; Li et al., 2021). For instance, all but 2 are associated with negative peak currents detected by GLD360. The short rise time suggests a fast streamer discharge as expected for NBEs (Rison et al., 2016), and at the top of clouds where negative NBEs are found (Wu

et al., 2013). NBEs are generally associated with regions of strong convection and high cloud tops (Jacobson & Heavner, 2005; Karunarathna et al., 2015; Wiens et al., 2008; Wu et al., 2012), as we also find here.

Thunderstorm clouds are generally assumed to have an upper positive charge region shielded by a negative charge layer above. Blue corona discharges at the cloud tops and blue jets are thought to be discharges between the upper positive and the screening layers. The radiosonde (Figure S1 in the Supporting Information S1) suggests that there was a strong wind shear above 7.5 km and the wind speed increased rapidly from 13.7 to 17.02 km altitude with strong winds at the cloud tops (70 knots/36 ms<sup>-1</sup>), which, in turn, suggests the presence of turbulence and strong mixing of charge layers (Riousset et al., 2010). Furthermore, weak electrification could occur in the anvils without the presence of supercooled water via the non-inductive charge mechanism (Dye & Bansemer, 2019). These conditions would explain why 2 of 14 discharges correlated with positive polarity strokes of high peak currents (64,102 kA) (Table S1 in the Supporting Information S1), rather than with negative strokes, as expected.

We note that 7 out of the 14 blue corona discharges are followed by UV pulses of less than 1 ms duration. The shape of the pulses and their temporal relation to the blue peaks suggest they are elves generated by the electromagnetic pulse emitted by the blue corona discharge current, as argued in Neubert et al. (2021) and predicted in Marshall (2012). They are marked as “double” in Table S1 in the Supporting Information S1, and are associated with the highest currents detected by GLD360. Elves are usually associated with lightning strokes with high peak currents, short rise times and of both polarities (Barrington-Leigh & Inan, 1999; van der Velde & Montanyà, 2016). The presence of the UV pulses suggests that the corona discharge currents are able to generate elves when the current is of sufficient magnitude.

### Data Availability Statement

Supplementary ASIM data and VAISALA GLD360 lightning data can be obtained by request from the Data tab on <https://asdc.space.dtu.dk>. Earth Networks lightning data supporting this research are freely available for research purposes. To obtain access to the data, contact Steve Prinzivalli ([sprinzivalli@earthnetworks.com](mailto:sprinzivalli@earthnetworks.com)). Data is not openly available because it is proprietary and requires an NDA to be signed before being distributed. Atmospheric sounding data are available at <http://weather.uwyo.edu/upperair/sounding.html>. Himawari satellite data was supplied by the P-Tree System, Japan Aerospace Exploration Agency (JAXA) at <https://www.eorc.jaxa.jp/ptree/index.html> and can be accessed after user registration at [https://www.eorc.jaxa.jp/ptree/registration\\_top.html](https://www.eorc.jaxa.jp/ptree/registration_top.html). The radar data was provided by the Australian Bureau of Meteorology <http://www.openradar.io/>. Both ASIM data from <https://asdc.space.dtu.dk/> and the radar data used to generate the figures have been deposited in the data repository <https://doi.org/10.5281/zenodo.5222102>.

### Acknowledgments

KD acknowledges fruitful discussions with Hugh Christian. The authors thank VAISALA for the GLD360 lightning data. The authors thank Earth Networks for the ENTLN lightning data. ASIM is a mission of the European Space Agency (ESA) and is funded by ESA and by national grants of Denmark, Norway and Spain. The science analysis is supported by: the European Research Council grant n. 320839, the Research Council of Norway contracts 223252/F50 (CoE/BCSS), and the Ministerio Ciencia e Innovacion grant ESP 2017- 86263-C4. This project has received funding from the European Union's Horizon 2020 research and innovation programme under the Marie Skłodowska-Curie grant agreement 722337.

### References

- Barrington-Leigh, C. P., & Inan, U. S. (1999). Elves triggered by positive and negative lightning discharges. *Geophysical Research Letters*, 26(6), 683–686. <https://doi.org/10.1029/1999GL900059>
- Bates, B. C., Dowdy, A. J., & Chandler, R. E. (2017). Classification of Australian thunderstorms using multivariate analyses of large-scale atmospheric variables. *Journal of Applied Meteorology and Climatology*, 56(7), 1921–1937. <https://doi.org/10.1175/JAMC-D-16-0271.1>
- Bessho, K., Date, K., Hayashi, M., Ikeda, A., Imai, T., Inoue, H., et al. (2016). An introduction to Himawari-8/9- Japan's new-generation geostationary meteorological satellites. *Journal of the Meteorological Society of Japan. Ser. II*, 94(2), 151–183. <https://doi.org/10.2151/jmsj.2016-009>
- Chanrion, O., Neubert, T., Lundgaard Rasmussen, I., Stoltze, C., Tcherniak, D., Jessen, N. C., et al. (2019). The Modular Multispectral imaging array (MMIA) of the ASIM payload on the international space station. *Space Science Reviews*, 215(4). <https://doi.org/10.1007/s11214-019-0593-y>
- Chanrion, O., Neubert, T., Mogensen, A., Yair, Y., Stendel, M., Singh, R., & Siingh, D. (2017). Profuse activity of blue electrical discharges at the tops of thunderstorms. *Geophysical Research Letters*, 44(1), 496–503. <https://doi.org/10.1002/2016GL071311>
- Chou, J. K., Hsu, R. R., Su, H. T., Chen, A. B. C., Kuo, C. L., Huang, S. M., et al. (2018). ISUAL-observed blue luminous events: The associated sferics. *Journal of Geophysical Research: Space Physics*, 123(4), 3063–3077. <https://doi.org/10.1002/2017JA024793>
- Chou, J. K., Kuo, C. L., Tsai, L. Y., Chen, A. B., Su, H. T., Hsu, R. R., et al. (2010). Gigantic jets with negative and positive polarity streamers. *Journal of Geophysical Research*, 115(A7), 1–13. <https://doi.org/10.1029/2009JA014831>
- Christian, H. J., Blakeslee, R. J., & Goodman, S. J. (1989). The detection of lightning from geostationary orbit. *Journal of Geophysical Research*, 94(D11), 329–337. <https://doi.org/10.1029/jd094id11p13329>
- Dye, J. E., & Bansemer, A. (2019). Electrification in Mesoscale updrafts of deep stratiform and anvil clouds in Florida. *Journal of Geophysical Research: Atmospheres*, 124(2), 1021–1049. <https://doi.org/10.1029/2018JD029130>
- Jacobson, A. R., & Heavner, M. J. (2005). Comparison of narrow bipolar events with ordinary lightning as proxies for severe convection. *Monthly Weather Review*, 135(4), 1354–1363. <https://doi.org/10.1175/MWR3342.1>
- Karunarathna, N., Marshall, T. C., Stolzenburg, M., & Karunarathne, S. (2015). Narrow bipolar pulse location compared to thunderstorm radar echo structure. *Journal of Geophysical Research: Atmospheres*, 120(22), 11–690. <https://doi.org/10.1038/175238c0>



- Krehbiel, P. R., Rioussel, J. A., Pasko, V. P., Thomas, R. J., Rison, W., Stanley, M. A., & Edens, H. E. (2008). Upward electrical discharges from thunderstorms. *Nature Geoscience*, *1*(4), 233–237. <https://doi.org/10.1038/ngeo162>
- Kuo, C. L., Chou, J. K., Tsai, L. Y., Chen, A. B., Su, H. T., Hsu, R. R., et al. (2009). Discharge processes, electric field, and electron energy in ISUAL recorded gigantic jets. *Journal of Geophysical Research*, *114*(4), 1–10. <https://doi.org/10.1029/2008JA013791>
- Laroche, P., Betz, H. D., & Schumann, U. (2009). *Lightning: Principles, instruments and applications: Review of modern lightning research*. Springer. <https://doi.org/10.1007/978-1-4020-9079-0>
- Li, D., Luque, A., Gordillo-Vázquez, F. J., Liu, F., Lu, G., Neubert, T., et al. (2021). Blue flashes as counterparts to narrow bipolar events: The optical signal of shallow in-cloud discharges. *Journal of Geophysical Research: Atmospheres*, *126*(13). <https://doi.org/10.1029/2021jd035013>
- Liu, F., Zhu, B., Lu, G., Lei, J., Shao, J., Chen, Y., et al. (2021). Meteorological and electrical conditions of two mid-latitude thunderstorms producing blue discharges. *Journal of Geophysical Research: Atmospheres*, *126*(8), 1–13. <https://doi.org/10.1029/2020jd033648>
- Liu, F., Zhu, B., Lu, G., Qin, Z., Lei, J., Peng, K. M., et al. (2018). Observations of blue discharges associated with negative narrow bipolar events in active deep convection. *Geophysical Research Letters*, *45*(6), 2842–2851. <https://doi.org/10.1002/2017GL076207>
- Liu, N., McHarg, M. G., & Stenbaek-Nielsen, H. C. (2015). High-altitude electrical discharges associated with thunderstorms and lightning. *Journal of Atmospheric and Solar-Terrestrial Physics*, *136*, 98–118. <https://doi.org/10.1016/j.jastp.2015.05.013>
- Lyons, W. A., Nelson, T. E., Armstrong, R. A., Pasko, V. P., & Stanley, M. A. (2003). Upward electrical discharges from thunderstorm tops. *Bulletin of the American Meteorological Society*, *84*(4), 445–454. <https://doi.org/10.1175/BAMS-84-4-445>
- Marchand, M., Hilburn, K., & Miller, S. D. (2019). Geostationary lightning mapper and Earth networks lightning detection over the contiguous United States and dependence on flash characteristics. *Journal of Geophysical Research: Atmospheres*, *124*(21), 11552–11567. <https://doi.org/10.1029/2019JD031039>
- Marshall, R. A. (2012). An improved model of the lightning electromagnetic field interaction with the D-region ionosphere. *Journal of Geophysical Research*, *117*(3), 1–15. <https://doi.org/10.1029/2011JA017408>
- Neubert, T., Chanrion, O., Heumesser, M., Dimitriadou, K., Husbjerg, L., Rasmussen, I. L., et al. (2021). Observation of the onset of a blue jet into the stratosphere. *Nature*, *589*(7842), 371–375. <https://doi.org/10.1038/s41586-020-03122-6>
- Neubert, T., Østgaard, N., Reglero, V., Blanc, E., Chanrion, O., Oxborrow, C. A., et al. (2019). The ASIM mission on the international space station. *Space Science Reviews*, *215*(2). <https://doi.org/10.1007/s11214-019-0592-z>
- Rioussel, J. A., Pasko, V. P., Krehbiel, P. R., Rison, W., & Stanley, M. A. (2010). Modeling of thundercloud screening charges: Implications for blue and gigantic jets. *Journal of Geophysical Research*, *115*(A1). <https://doi.org/10.1029/2009ja014286>
- Rison, W., Krehbiel, P. R., Stock, M. G., Edens, H. E., Shao, X. M., Thomas, R. J., et al. (2016). Observations of narrow bipolar events reveal how lightning is initiated in thunderstorms. *Nature Communications*, *7*, 1–12. <https://doi.org/10.1038/ncomms10721>
- Said, R. K., Cohen, M. B., & Inan, U. S. (2013). Highly intense lightning over the oceans: Estimated peak currents from global GLD360 observations. *Journal of Geophysical Research: Atmospheres*, *118*(13), 6905–6915. <https://doi.org/10.1002/jgrd.50508>
- Said, R. K., & Murphy, M. J. (2016). GLD360 upgrade: Performance analysis and applications. In *24th International lightning detection conference (lc)*.
- Soler, S., Pérez-Invernón, F. J., Gordillo-Vázquez, F. J., Luque, A., Li, D., Malagón-Romero, A., et al. (2020). Blue optical observations of narrow bipolar events by ASIM suggest corona streamer activity in thunderstorms. *Journal of Geophysical Research: Atmospheres*, *125*(16). <https://doi.org/10.1029/2020JD032708>
- Stolzenburg, M., Rust, W. D., & Marshall, T. C. (1998). Electrical structure in thunderstorm convective regions 2. Isolated storms. *Journal of Geophysical Research*, *103*(D12), 14079–14096. <https://doi.org/10.1029/97JD03547>
- Tilles, J. N., Liu, N., Stanley, M. A., Krehbiel, P. R., Rison, W., Stock, M. G., et al. (2019). Fast negative breakdown in thunderstorms. *Nature Communications*, *10*(1), 1–12. <https://doi.org/10.1038/s41467-019-09621-z>
- van der Velde, O. A., & Montanyà, J. (2016). Statistics and variability of the altitude of elves. *Geophysical Research Letters*, *43*(10), 5467–5474. <https://doi.org/10.1002/2016GL068719>
- Wescott, E. M., Sentman, D. D., Osborne, D. L., Hampton, D. L., & Heavner, M. J. (1995). Preliminary results from the Sprites94 aircraft campaign: 2. Blue jets. *Geophysical Research Letters*, *22*(10), 1205–1208. <https://doi.org/10.1029/95gl00582>
- Wiens, K. C., Hamlin, T., Harlin, J., & Suszcynsky, D. M. (2008). Relationships among Narrow Bipolar Events, “total” lightning, and radar-inferred convective strength in Great Plains thunderstorms. *Journal of Geophysical Research*, *113*, 1–31. <https://doi.org/10.1029/2007JD009400>
- Wu, T., Dong, W., Zhang, Y., Funaki, T., Yoshida, S., Morimoto, T., et al. (2012). Discharge height of lightning narrow bipolar events. *Journal of Geophysical Research*, *117*(D5), 1–13. <https://doi.org/10.1029/2011JD017054>
- Wu, T., Takayanagi, Y., Yoshida, S., Funaki, T., Ushio, T., & Kawasaki, Z. (2013). Spatial relationship between lightning narrow bipolar events and parent thunderstorms as revealed by phased array radar. *Geophysical Research Letters*, *40*(3), 618–623. <https://doi.org/10.1002/grl.50112>
- Zipser, E. J., & Lutz, K. R. (1994). The vertical profile of radar reflectivity of convective cells: A strong indicator of storm intensity and lightning probability? *Monthly Weather Review*, *122*, 1751–1759. [https://doi.org/10.1175/1520-0493\(1994\)122<1751:tvporr>2.0.co;2](https://doi.org/10.1175/1520-0493(1994)122<1751:tvporr>2.0.co;2)